Available online at
https://journal.uitm.edu.my/ojs/index.php/MJCET

e-ISSN: 2682-8588

Malaysian Journal of Chemical Engineering & Technology 8(2) 2025, 223–239

Malaysian Journal of Chemical Engineering and Technology

Evaluating the feasibility of chitosan-based carbon quantum dots in xerogel matrix for CO_2 removal

Nur Ainaa Mohd Hasyim Chan[1], Norhusna Mohamad Nor[2*]

[1,2]*Chemical Engineering Studies, Universiti Teknologi MARA Cawangan Pulau Pinang, 13500 Permatang Pauh, Pulau Pinang, Malaysia*

ARTICLE INFO

Article history:
Received 13 January 2025
Revised 27 October 2025
Accepted 14 December 2025
Online first
Published 31 December 2025

Keywords:
Adsorption
Carbon dioxide
Carbon quantum dots (CQDs)
Chitosan
Shrimp shells
Xerogel

DOI:
10.24191/mjcet.v8i2.4613

ABSTRACT

This study investigates the feasibility of using xerogel as a support matrix to stabilise chitosan-based carbon quantum dots (CCQDs) for CO_2 adsorption. After being hydrothermally treated for 24 hours at 180°C, CCQDs were immobilised in xerogel matrices with different ratios of CCQDs to solution. Tests for CO_2 adsorption were carried out at 30°C, 100 mL/min flow rate, and 5% CO_2 concentration. The CCQD-X 1:50 sample had the maximum adsorption capacity, at 80.28 mg/g. The existence of hydroxyl, carbonyl, and C–O functional groups that promote CO_2 binding was verified by FTIR analysis. According to TGA measurements, CCQD-X 1:1 demonstrated exceptional thermal stability by retaining the largest residual mass of 40% at 950°C. With a surface area of 0.1864 m^2/g for CCQD-X 1:50, BET analysis validated mesoporous properties, while FESEM pictures showed a heterogeneous xerogel surface shape. CHNS elemental analysis confirmed that nitrogen and sulfur were successfully incorporated, increasing the adsorbent's affinity for CO_2 through polar and basic surface functions. Overall, the results show that CCQDs supported by xerogel have better stability and functional characteristics, which makes them a viable and sustainable adsorbent for effective CO_2 collection applications.

1. INTRODUCTION

Global CO_2 emissions have reached critical levels due to anthropogenic activity, mainly the burning of fossil fuels and deforestation, which has accelerated climate change and its effects, such as rising global temperatures and a rise in the frequency of extreme weather events. Despite this, there has been no decrease in emissions from major industries, transportation, energy, and agriculture between 1990 and 2018, mostly as a result of slower adoption of low-carbon alternatives and persisting consumer demand (Bahman et al., 2023; Lamb et al., 2021). Emissions have significantly increased because of the continued industrialisation of Eastern and Southern Asian countries, particularly China and India. Due primarily to the burning of fossil fuels, this trend helped the world's greenhouse gas emissions reach about 58 Gt CO_2 equivalent in 2018 (Minx et al., 2021). Despite moderate decarbonisation in North America and Europe, global emissions are still rising, underscoring the urgent need for policy changes (Friedlingstein et al., 2010; Minx et al., 2021). The goal of the Paris Agreement to limit global warming to less than 2°C has sped up the search for sustainable CO_2 capture techniques. Conventional techniques, like amine scrubbing and membrane

[2*]Corresponding author. *E-mail address*: norhusna8711@uitm.edu.my
https://doi.org/10.24191/mjcet.v8i2.4613

separation, are usually too costly, energy-intensive, and inefficient for widespread use. This encourages the hunt for alternative materials. Carbon quantum dots (CQDs) represent a practical, economical, and environmentally friendly alternative for enhancing capture efficiency, particularly when derived from bio-waste sources such as prawn shells.

Carbon quantum dots (CQDs) are nanoscale particles (less than 10 nm) with high surface area, tunable surface chemistry, and exceptional thermal stability. Because of these properties, they are very versatile, particularly when it comes to CO_2 capture, where their surfaces can be functionalised to increase adsorption capacity and selectivity. Chitosan, a naturally occurring biopolymer derived from prawn shells, is a great, eco-friendly precursor for the synthesis of CQDs. Among the many beneficial properties of chitosan-derived CQDs are their high surface functional group count and enhanced biocompatibility. Moreover, even in low-cost and sustainable production scheme, the natural characteristic of chitosan including high nitrogen content and high hydrogen bonding can be directly applied to optimise the CO_2 adsorption characteristics and selectivity of the obtained CQDs. Heteroatomic doping (N, S and O) of CQDs also enhances their CO_2 adsorption capacity by changing their surface characteristics and porosity. Thiourea (CH_4N_2S) is a good source of dopants, and it is used as a co-introducer of nitrogen and sulfur which improves the surface chemistry, thereby raising the capacity and selectivity of the CO_2 collection (Cui et al., 2022; Nazir et al., 2021). Meanwhile, potassium hydroxide (KOH) is used as an activator and significantly increases the surface area of the CQDs and personalises the pore structure, making CQDs more efficient as CO_2 adsorbents (Chen et al., 2023; Helmi et al., 2023). These adjustments are effective synergies such that they help in maximizing the structural and functional properties of CQDs that make it a viable platform to capture CO_2. Nevertheless, a significant issue arises when the CQDs are freeze-dried since they are likely to accumulate leading to low adsorption capacity and instability. We immobilised the CQDs in a xerogel matrix to reduce this. This scaffold has provided a high surface area, porous, stable structure which prevents aggregation and facilitates more effective CO_2 collection which enhances the overall adsorption performance.

Xerogels are solid materials, which offer good adsorbents due to their high porosity and huge surface area. This has been made possible by their large surface area that provides a large number of active sites on the gas-solid interactions which are critical to capture CO_2 and their network of interconnected pores, which facilitates the diffusion of gases. Also, xerogels exhibit outstanding structural stability (in extreme circumstances) and this guarantees reliable performance in the long term. Fig. 1 illustrates the process used to make xerogels; a sol is polymerised and cross-linked to form a gel, and the end product is obtained by ambient pressure drying. It is primarily the consequence of this process that gives them their solid, permeable structure and supports their functioning. It is worth noting that the xerogel-based adsorbents have a high potential of enhancing CO_2 capture systems because they have been shown to be effective in the present-day gas capture technology.

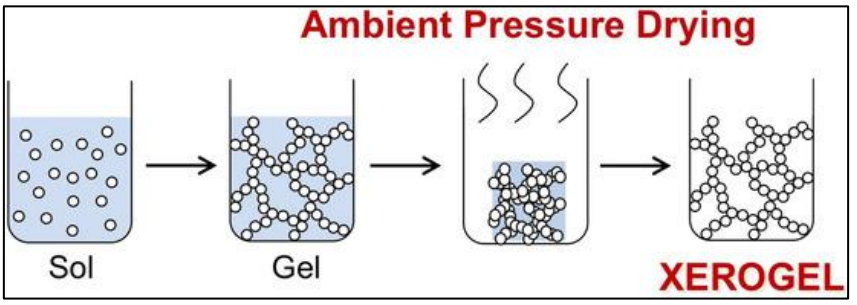

Fig. 1. Schematic representation of xerogel formation through ambient pressure drying

Source: Shimizu et al., 2017

https://doi.org/10.24191/mjcet.v8i2.4613

Aguilar-Maruri et al. (2024) justified our assertion because the study prepared organic xerogels using resorcinol and formaldehyde and achieved a maximum adsorption capacity of 325mg/g of metformin at pH 11. The study conducted by Yilmaz demonstrated that silica-based xerogels have a capacity of 1666.67 mg/g to remove methylene blue in vitro xerogels, which means that this type of xerogel is highly efficient in the adsorption of dyes (SEZGIN, 2022). Li et al. found out exclusive structural aspects and wastewater-treatment capability in superhydrophobic phenolic xerogels in the adsorption of organic pollutants (Li et al., 2022). The immobilisation of CQDs onto a xerogel scaffold greatly increases the adsorption capacity of CQDs because the xerogel provides a favourable scaffold that facilitates the interaction with the CO_2 moles to their maximum. It is hoped that this mixture of CQDs and xerogels will offer higher efficiency and durability of the adsorbent.

The development of new nanomaterials, including CQDs, has been necessitated by the urgent need to find effective ways of capturing carbon to reduce climatic change. The advantage of CQDs in the CO_2 capture is high surface-volume ratio and controllable surface chemistry. Nevertheless, the vast majority of CQD synthesis is based on synthetic and petrochemical feedstock, which also compromises the green nature of the technology and makes it more expensive. This highlights the strong potential for producing CQDs from waste biomass and abundant renewable resources. The best precursor is shrimp-shell-derived chitosan, which is a nitrogen-containing, sustainable compound that could be improved to increase CO_2 adsorption. Also, CQDs may be afflicted by the problem of handling, aggregation, and recyclability. It is possible to incorporate CQDs into a solid porous support, like xerogels, to give a high-surface-area matrix stable to aggregation, and the diffusion of gases.

This study investigates the performance of chitosan-derived CQDs immobilised in xerogel to capture CO_2. Based on the utilisation of shrimp-shell biowaste, this study meets the requirement of sustainable capture technology. The main goals are to: (1) assess the chitosan-CQD-xerogel composite's CO_2 adsorption effectiveness; and (2) systematically investigate how heteroatom doping (with N, S, and O) improves the adsorption capacity and selectivity of the CQDs. The main goal is to determine whether this integrated, environmentally friendly platform is a practical and affordable way to reduce CO_2 emissions.

2. METHODOLOGY

2.1 Chemicals

In this study, shrimp shells were purchased from a local shop. Chitosan was extracted from shrimp shells using hydrochloric acid, HCl (37%, Merck), sodium hydroxide, NaOH (98%, Merck), and ethanol, C_2H_6O (95%, Merck). Thiourea, CH_4N_2S (99%, Sigma Aldrich) along with potassium hydroxide, KOH (85%, Merck) were used to enhance the chitosan-based CQDs during hydrothermal synthesis. For the xerogel synthesis, sodium alginate, $(C_6H_7NaO_6)$ n (R&M Chemicals), calcium carbonate, $CaCO_3$ (R&M Chemicals), and glucono delta-lactone, GDL (DChemie) were used. CO_2 gas (10 v/v% CO_2 in N_2), and N_2 gas (99.99%) were supplied by Alpha Gas Solution and were used for CO_2 sorption experiments.

2.2 Hydrothermal synthesis of chitosan-based shrimp shells CQDs

The extraction of chitosan from shrimp shells waste followed Boudouaia et al. (2019). Chitosan-based CQDs (CCQDs) were synthesised using the extracted chitosan-derived shrimp shells through a hydrothermal method. The process involved mixing 1 g of chitosan, 1 g of thiourea, and 3 g of KOH as doping agents to enhance the functional properties of the CQDs. The powdered mixture was dissolved in 100 mL of deionised water and stirred for 30 min. The resulting solution was transferred to a 200 mL Teflon-lined container, which was then placed inside a stainless-steel autoclave. The hydrothermal procedure was carried out for 24 hours at 180°C in a Memmert UNE200 oven (Paul & Kurian, 2021). The liquid was allowed to cool to room temperature following the reaction. The mixture was centrifuged for

https://doi.org/10.24191/mjcet.v8i2.4613

20 min at 2000 rpm in order to extract the CCQDs from the hydrochar. After that, the suspension's CCQDs were filtered out.

2.3 Synthesis of xerogel immobilised CCQDs

As indicated in Table 1, 1 g of sodium alginate was dissolved in a solution made with different volumes of CCQDs suspension to produce the xerogels immobilised CCQDs. For full dissolution, the mixture was left to stand for a full day. A sol (first colloidal suspension) was then formed by adding 0.2 g of $CaCO_3$ to the solution and stirring it at 450 rpm to induce hydrolysis and condensation. After the sol was homogeneous, 0.3 g of GDL was added to dissolve the $CaCO_3$ and liberate the Ca^{2+} ions, which then formed a gel by cross-linking with the alginate. Xerogels formed by aging the gel at room temperature, transferring it into silicone moulds, and then drying it in an oven set at 80°C for 24 hours (Alias et al., 2022; Deana et al., 2023). Although the overall procedure was in line with earlier research, the author conducted numerous trial-and-error experiments to optimise certain parameter selections, such as the ratio of components and suspension volumes, in order to achieve a stable and uniform xerogel formation. In this work, four types of xerogel samples were prepared for analysis: those immobilised with three different suspensions (2 mL, 10 mL, and 100 mL of CCQDs suspension) and one using freeze-dried CQDs.

Table 1. Preparation methods and abbreviations of CCQDs samples

CCQDs phase	Sample abbreviation	Preparation method
Aqueous suspensions	CCQD-X 1:50	Prepared using 2 mL of CCQDs suspension in a total of 100 mL solution
Aqueous suspensions	CCQD-X 1:10	Prepared using 10 mL of CCQDs suspension in a total of 100 mL solution
Aqueous suspensions	CCQD-X 1:1	Prepared using 100 mL of CCQDs suspension with no added distilled water
Freeze-dried sample	FD CCQD-X 1:50	Prepared using 2 g of freeze-dried CCQDs in a total of 100 mL solution

Source: Author's own data

2.4 CO_2 adsorption experiment

The performance of CCQD-X adsorbents in determining the optimal doping ratio was evaluated using a custom-designed CO_2 adsorption setup as shown in Fig. 2. A 0.5 g sample of the CCQD-X adsorbents was placed at the centre of a stainless-steel column, 250 mm long and 9.525 mm in diameter, supported by 0.3 g of borosilicate glass wool.

At a temperature of 30°C, a controlled CO_2/N_2 gas mixture was passed through the column at a constant flow rate of 100 mL/min, with the gas composition regulated by a Dwyer flow meter and CO_2 concentration of 5%. The inlet and outlet CO_2 concentrations were continuously monitored using a portable gas analyser equipped with an electrochemical sensor calibrated for syngas composition (MRU-Optima 7). Continuous CO_2 readings were taken every minute, and the experiment was stopped when the concentration ratio (Ci/Co) hit 0.95, which denotes saturation. Eq. (1) was used to determine the CCQD-X adsorbents' adsorption capacity.

$$q = \frac{Q_f t_t y_f}{m_c} \tag{1}$$

where q is the adsorption capacity of the adsorbent in milligrams per gram, Q_f is the volumetric feed flow rate measured in millilitres per minute, y_f indicates the mole fraction of the adsorbate expressed in milligrams per millilitre, t_t represents the breakthrough time in minutes, m_c and is the mass of the adsorbent in grams.

https://doi.org/10.24191/mjcet.v8i2.4613

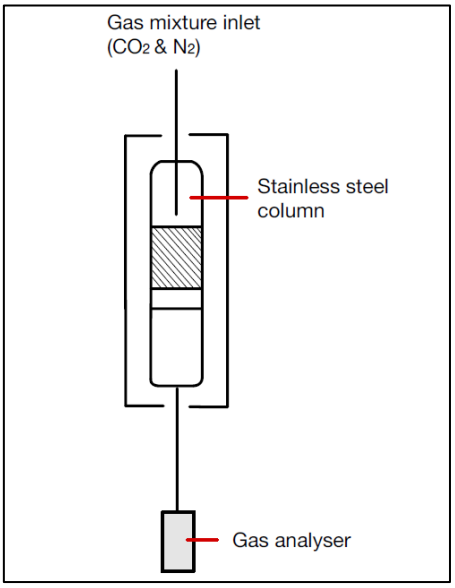

Fig. 2. Schematic diagram of CO_2 adsorption setup

Source: Author's own illustration

2.5 Characterisation

Several analytical techniques were used in characterising CQD-X. The chemical bonds and functional groups were identified using Thermo Scientific Nicolet iS10 FTIR instrument and the following changes were found that enhance the interaction of CO_2. According to the Brunauer-Emmett-Teller (BET) approach and the ASAP 2020 micromeritics model, increased surface areas are associated with an increased CO_2 uptake, which is also consistent with the recent research on activated carbons and zeolites (Gautam & Sahoo, 2022; Kim & Kim, 2023). Thermogravimetric Analysis (SDT 0600) was used to measure thermal stability, whereas Scanning Electron Microscopy (FESEM, Nova Nanosem 450) demonstrated the surface structure on which adsorption sites were located (Gautam & Sahoo, 2022). Only the CCQD-X 1:50 sample was investigated in certain analyses as it showed the highest CO_2 adsorption capacity and performance in general, so it became the subject of further investigation. Making emphasis on this sample, we can comprehend better the structural and chemical factors that make CCQD-X 1:50 possess such outstanding adsorption.

3. RESULTS AND DISCUSSION

3.1 Physical surface characteristics and morphology

BET surface area analysis measures surface area and porosity that is important in CO_2 adsorption. The analysis includes quantitative information regarding certain surface area and pore volume, which will allow us to know the impact that surface change has on performance. The BET data indicate the effect of the dopants on the porosity and surface area which changes adsorbent behaviour. Fig. 3 demonstrates the BET isotherm of CCQD-X 1:50 sample. Table 2 presents detailed measurements of single-point surface area, BET area, Langmuir area, t-plot micropore area, and t-plot micropore volume.

https://doi.org/10.24191/mjcet.v8i2.4613

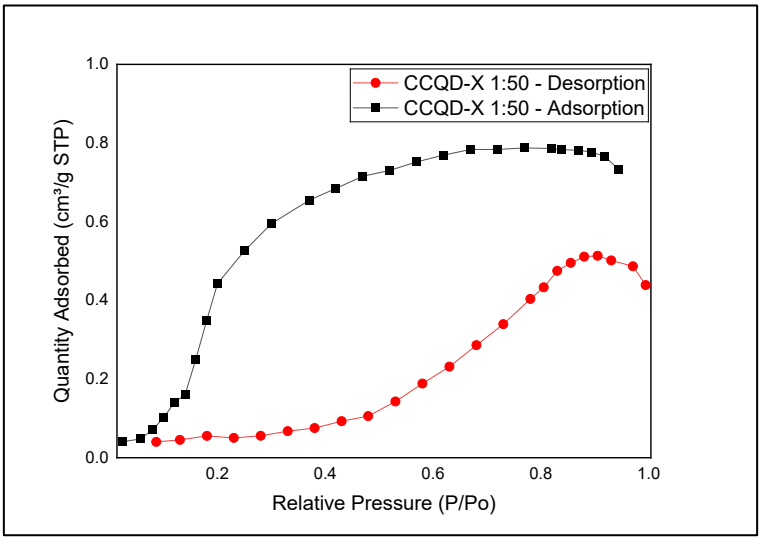

Fig. 3. BET isotherm plot for CCQD-X 1:50 sample

Source: Author's own data

Table 2. Surface Area and Pore Volume of CCQD-X 1:50

Single point surface area at P/Po, m^2/g	BET Surface Area, m^2/g	Langmuir Surface Area, m^2/g	t-Plot Micropore Area, m^2/g	t-Plot micropore volume, cm^3/g
0.1589	0.1864	0.2617	0.2601	0.000156 cm^3/g

Source: Author's own data

Its isotherm is type IV, with a distinct hysteresis loop which is characteristic of mesoporous materials with a pore size of between 2 and 50 nm. Capillary condensation within the mesopores is suggested by the hysteresis loop that exists between the adsorption and desorption branches. Smaller pore filling causes a slow increase in nitrogen uptake at lower relative pressures, which is followed by a sharp increase at higher pressures because of capillary condensation in bigger mesopores. Due to pore geometry and surface tension effects, nitrogen gas evaporates at a lower pressure than it condenses, as seen by the hysteresis loop of the desorption branch, which is characteristic of slit-shaped or cylindrical pores. The BET theory and t-Plot method were used to determine the surface area and pore characteristics of CQD-X 1:50. The BET surface area is 0.1864 m^2/g and t-plot area of micropores is 0.2601 m^2/g which means that the material has mesopores and micropores that are significant in CO_2 capture. On the contrary, Mahdi et al. (2024) stated that the surface area of activated carbon is significantly higher (868 m^2/g), the pore size is 1.7532 nm, and the pore volume is 0.3805 m^3/g. The gel-drying results in blockage of pores and structural shrinkage with decrease in surface area, pore size and volume in xerogel samples. For example, the palm kernel shell biochar (PKSB) has 355.7066 m^2/g surface, pore size 2.0376 nm and volume 0.1820 cm^3/g whereas the xerogel counterpart (PKSBX) has 29.4535 m^2/g, 4.6203 nm and 0.0295 m^3/g (Mahdi et al., 2024). This comparison shows that while xerogel structures such as CQD-X 1:50 possess a sufficient surface area for targeted applications, their specific surface area is typically lower than that of highly porous materials like activated carbon. This discrepancy is a direct consequence of the structural shrinkage and pore collapse inherent to the gelation and ambient pressure drying processes.

https://doi.org/10.24191/mjcet.v8i2.4613

Field Emission Scanning Electron Microscopy (FESEM) is used to examine the surface morphology and structural characteristics of the CCQD-X, focusing on the best-performing adsorbent. As shown in Fig. 4, the morphology observed in the FESEM results is comparable with the physical surface characteristics from the BET research. To ascertain how the structural components impact the CCQD-X's capacity to absorb CO_2 and to establish a relationship between physical attributes and adsorption performance, this visual study is required.

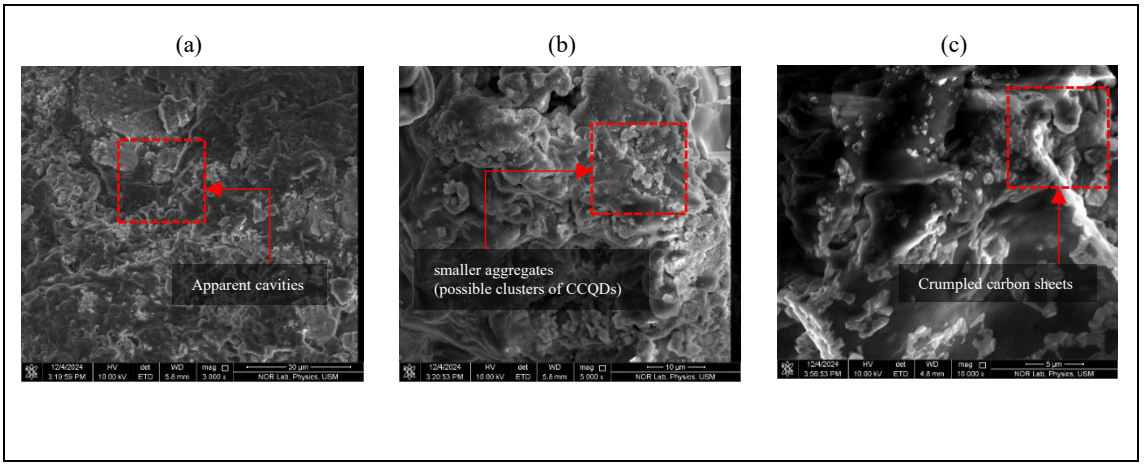

Fig. 4. FESEM images of CCQD-X 1:50 from various magnifications: a) 3000x; b) 5000x; c) 10000x

Source: Author's own data

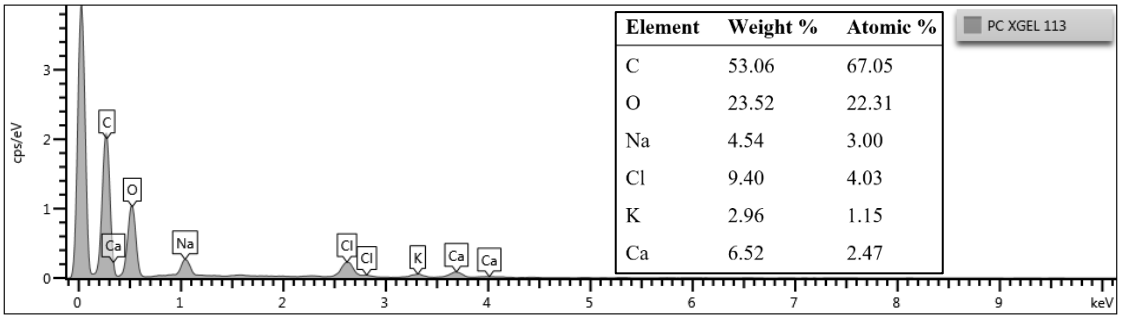

Element	Weight %	Atomic %
C	53.06	67.05
O	23.52	22.31
Na	4.54	3.00
Cl	9.40	4.03
K	2.96	1.15
Ca	6.52	2.47

Fig. 5. Quantitative analysis of the energy dispersive X-ray (EDX) analysis on CCQD-X 1:50 sample

Source: Author's own data

The CCQD-X 1:50 micrographs show a very irregular and heterogeneous surface at all magnifications. The xerogel matrix structure at 3000× indicates uneven distribution of particles by having a mound-and-valley geometry with apparent cavities. At the 5000× scale, smaller aggregates or clusters of CCQDs are observed, and the surface takes the topology of a network with numerous protrusions and hollows. The surface is highly rough and twisted at 10,000×, and groups of nanoparticles, holes and crumpled sheets of carbon can be observed. In other areas, there are extensive planar terrains that are similar to layers of piled

https://doi.org/10.24191/mjcet.v8i2.4613

carbonaceous. These structural characteristics indicate that N/S/O doping of the CCQDs changes the xerogel microstructure to form an irregular, accessible surface that enables the catalysis of gas-solid interactions during CO_2 adsorption. Although the FESEM image does not display well-defined mesopores, the observed surface irregularities and interparticle voids imply a texturally open framework that complements the BET findings, which indicate a mesoporous structure with considerable surface area.

There is prior research on such morphologies. For instance, RF xerogels are outlined by Aguilar-Maruri et al. (2024) to be "agglomerated in irregular shapes with smooth and striated faces, and acid-activated carbons were found to have "aggregated and rough surface morphology with interconnected particles forming surface pores" (Olasehinde & Abegunde, 2020). It is well known that these highly rough, clumped textures increase the adsorption area. According to Gong et al. (2025), rough surfaces coated with nanoparticles "effectively increase the specific surface area" of biochars. Similarly, xerogel-derived carbons frequently form sheet-like, porous networks, similar to the "sheet-like morphology" in N-doped carbon supports that correlates with high porosity reported by Hao et al. (2023).

The energy dispersive X-ray (EDX) analysis for the CCQD-X 1:50 sample is quantitatively analysed in Fig. 5, which gives the weight and atomic percentages of each element in the sample. Carbon (C), oxygen (O), sodium (Na), chlorine (Cl), potassium (K), and calcium (Ca) are the main elements found, according to the table. C and O are found to be significantly present, with weight percentages of 53.06% and 23.52%, respectively. The CQDs which are formed during the synthesis process from chitosan, are primarily responsible for the high carbon content. Numerous oxygen-containing functional groups, including hydroxyl (–OH), carbonyl (–C=O), and carboxyl (–COOH) groups, are probably present because of the oxidation of chitosan and its interaction with other synthetic materials. The weight percentages for the detection of sodium (Na) and chlorine (Cl) are 4.54% and 9.4%, respectively. The sodium alginate used to prepare the xerogel is probably the source of the sodium. The residuals from the thiourea or other synthesis chemicals may be the origin of the chlorine. Sodium alginate contributes to the porosity structure shown in the FESEM pictures by encasing the carbon quantum dots in a hydrogel network. The presence of potassium at 2.96% by weight is attributed to the use of KOH during the doping procedure. KOH is used as a strong base during CCQDs synthesis which facilitates deprotonation and cross-linking. This increases strength of particles and improves their functionality. Potassium also offers the surface basic sites to enhance the CO_2 adsorption. The calcium carbonate ($CaCO_3$), which is utilised in the manufacturing of the xerogel, provides 6.52 wt.% Ca. It is a pore former which releases CO_2 when it decomposes during the gelation process, forming a porous network that enhances surface area and adsorption capacity. The EDX analysis confirms that the following synthesis additives were included in the sample of CCQD-X 1:50. These materials are quite significant in determining the structure, the functionality, and the elemental composition of the adsorbent.

3.2 Thermal stability

Thermogravimetric analysis (TGA) is used to evaluate compositional variations and thermal stability of CCQD-X. The test demonstrates the resistance of the material to high temperatures and determines the loss of weight due to volatile components or decomposition. Fig. 6 shows TGA of CCQD-X 1:1, CCQD-X 1:10, CCQD-X 1:50, and FD CCQD-X 1:50 samples.

The TGA curves show three different weight-loss areas: moisture loss, decomposition of volatile matter, and degradation of fixed-carbon, which is also consistent with the results of the studies by Alias et al. The initial area, 70℃ - 100℃ indicates the evaporation of moisture. The lowest initial loss is observed in the CCQD-X 1:50 with the initial loss being 103.27°C. The second region, between 300°C and 700°C, is associated with the dissolution of volatile organics and gaseous emissions of the CCQDs and xerogel matrix. This area begins earlier in CCQD-X 1:50, and this means that it has less thermal stability because of its greater xerogel content.

https://doi.org/10.24191/mjcet.v8i2.4613

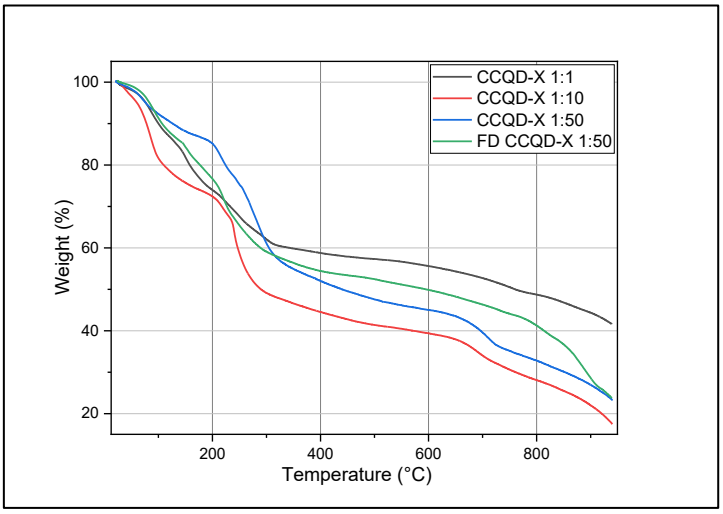

Fig. 6. Thermogravimetric analysis (TGA) curve of CCQD-X samples

Source: Author's own data

The thermal stability of the adsorbents was found to be composition dependent. Conversely, CCQD-X 1:1, and FD CCQD-X 1:50 starts to degrade at a higher temperature (342.94°C) with less loss of weight and is more stable. The dense structure of CCQD-X 1:1 is due to its large CCQDs ratio, which is probably one of the causes of its heat resistance. The freeze-dried FD CCQD-X 1:50 exhibits a clear degradation behaviour, which is indicative of variation in thermal behaviour reflecting altered CCQDs distribution and matrix interactions introduced by the freeze-drying process.

The last stage, at 700°C to 950°C, is due to the breakdown of fixed carbon. The highest content of CCQDs samples, namely, CCQD-X 1:1 and FD CQD-X 1:50 are more thermally stable. They are harder in structure and have few or smaller pores, which explains their constant degradation. CCQD-X 1:1 with the start temperature of 760.09°C and a residual weight of 40°C demonstrates a strong carbon skeleton. FD CCQD-X 1:50 follows closely at 729.76°C. Altogether, the TGA data reveal that the preparation procedure and CCQDs condition (aqueous suspension or freeze-drying) have a strong effect on thermal degradation.

The study by Alias et al. (2022) found that xerogel-based EFB release moisture sooner in the first region than raw EFB and hydrogel because xerogel was more crystalline. This high rate of crystallinity decelerates the absorption of moisture as the inter-molecular hydrogen bonds are substituted with the –OH functional groups. Hydroxyl groups loss and backbone disintegration of alginate resulted in more weight loss of xerogel. The same pattern is exhibited by the CCQD-X samples. The initial loss of moisture at 103.27°C was also seen in CCQD-X 1:50 that has the lowest content of CCQDs and a more xerogel-like structure. Greater crystallinity in xerogel-like structures results in premature release of moisture. It was also discovered in the investigation that samples based on xerogel lost more weight since they exhibit hydroxyl loss and degradation of the alginate. A sharp decrease in weight in the second region (300°C – 700°C) indicates the degradation of the xerogel structure and volatile organics. The fact that CCQD-X 1:50 begins to degrade earlier than samples with a higher CCQDs concentration point to a reduction in thermal stability, a trend analogous to the increased degradation observed in xerogel-based materials compared to their raw or hydrogel counterparts in prior research (Alias et al., 2022). This comparison highlights the importance of preparation methods in adjusting the thermal characteristics of materials for certain applications. The maximum temperature was 950℃, and thus, the degradation of CCQD-X is not fully developed. Noraini et al. (2022) discovered that xerogel biochar is completely degraded at 1189.97°C.

https://doi.org/10.24191/mjcet.v8i2.4613

3.3 Surface functional groups

Fourier Transform Infrared Spectroscopy (FTIR) provides vivid information on the functional groups and the chemical structure of CCQD-X. The method recognises individual chemical bonds that are developed when doping and identifies them by comparing the FTIR spectra of the various samples presented in Fig. 7. This discussion indicates that the doping will modify the chemical environment of CCQD-X, resulting in modification of its adsorption behaviour.

The FTIR spectra of CCQD-X have a number of functional groups that augment its adsorption capacity. The sharp peak at 3200–3600 cm^{-1} indicates the presence of hydroxyl (–OH) and amine (N–H) groups belonging to the chitosan structure, enhancing the hydrogen bonding with polar molecules like CO_2. The 2800–3000 cm^{-1} peaks are the result of aliphatic C–H stretching, which is used to indicate the chitosan backbone and perhaps the carbon-quantum dots. An apex of approximately 2300 cm^{-1} is related to CO_2 vibrations being adsorbed on the surface which proves the presence of CO_2 affinity, confirming its suitability for carbon capture applications (Alias et al., 2022). Oxidised quantum dots or carboxyl groups within the CQDs, produce carbonyl (C=O) groups that provide a very strong peak between 1650 and 1750 cm^{-1}, which increases dipole-dipole interactions. Unsaturated C=C bonds are represented as peaks in the 1600–1680 cm^{-1} range, which contributes to π–π interactions of adsorbates. Signal C–O– linkages indicative of alcohols or ethers at 1000–1300 cm^{-1}, which contributes to the adsorption of polar molecules. C–H bending vibrations in the 600–900 cm^{-1} range imply a graphitic structure and contains aromatic rings that facilitate the π–π stacking interactions beneficial for adsorbing various gaseous or aromatic compounds (Hannachi et al., 2019).

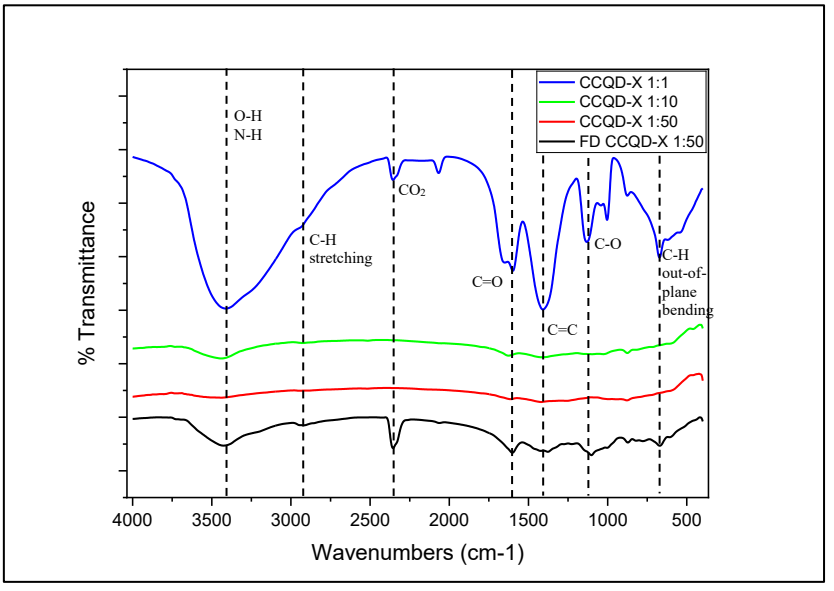

Fig. 7. FTIR spectra of CCQD-X with varying CCQDs suspensions and freeze-dried CCQDs

Source: Author's own data

https://doi.org/10.24191/mjcet.v8i2.4613

As Fig. 7 reveals, the spectra of some CCQD-X samples have distinct differences concerning the proportions of CCQDs suspension, and the state of the material (suspension or freeze-dried). The sample that has the highest concentration of CCQDs (100 mL) and is therefore named CCQD-X 1:1 presents the most clear and sharp peaks, a characteristic of a dense array of functional groups and a high-affinity interaction of CCQDs and alginate matrix. A broad, strong absorption in the 3200–3600 cm^{-1} region, characteristic of O–H stretching vibrations from hydroxyl groups. Other prominent peaks around 2900 cm^{-1} for C–H stretching and 1000–1200 cm^{-1} for C–O stretching, indicate functional groups that are associated to the alginate structure and the CCQDs. The freeze-dried CCQD-X 1:50 sample was next, but with less distinct peaks. Even though freeze-drying can result in slight aggregation of CCQDs, the O–H, C–H, and C–O groups remain preserved in the spectrum. The wider peaks indicate less homogenous dispersion of functional groups. In contrast, as shown in Fig. 8, progressively weaker peaks are shown by CCQD-X 1:10 and CCQD-X 1:50 samples, reflecting their low CCQDs content (10 mL and 2 mL).

The intermediate level of CCQDs in CCQD-X 1:10 shows stronger O–H and C–H peaks compared with CCQD-X 1:50, suggesting a higher level of dispersion and interaction. CCQD-X 1:10 sample has fewer functional groups, which are however more pronounced, and implies that there is some partial loss compared to the more concentrated CCQD-X 1:1. On the other hand, CCQD-X 1:50 shows the least distinct peaks, which shows that the low concentration of CCQDs decreases the structural homogeneity and functional group visibility, resulting in a significant decrease in functional groups. In general, the samples containing less CCQDs or freeze-dried CCQDs have broader, less distinct spectral features, likely due to aggregation, reduced uniformity, or a dilution effect. Conversely, at elevated concentrations of CCQDs, e.g. CCQD-X 1:1, functional groups are clearly defined. These results underscore the impact of the relation of the CCQDs to solution ratio as well as the physical state of the CCQDs to the structural and chemical characteristics of the xerogels (Kloos et al., 1999). Elemental analysis of CHNS determined the content of elements, and it gave an idea of the impact of the synthesis process on the distribution of the elements of carbon, hydrogen, nitrogen, and sulfur. These findings are associated with the occurrence and strength of functional groups in the FTIR spectra, as presented in Table 3 and further explain the chemical composition of the samples.

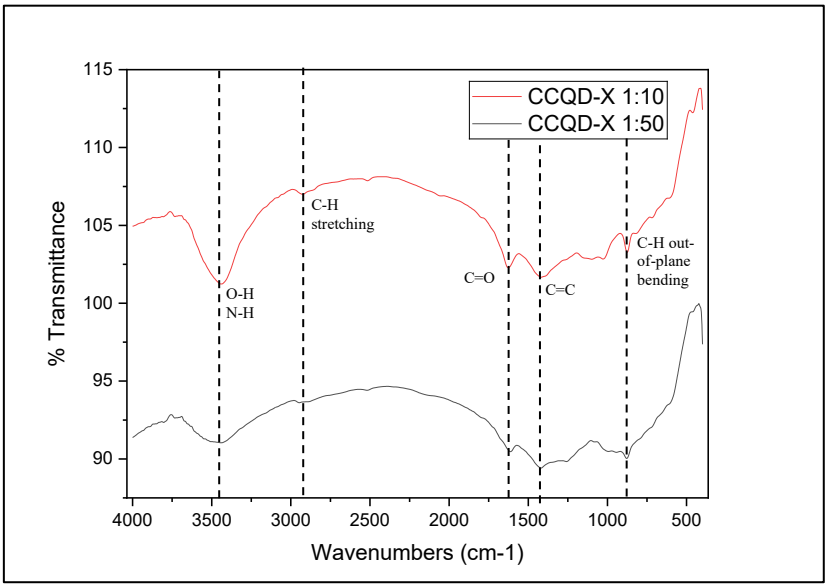

Fig. 8. Enlarged FTIR spectra of CCQD-X 1:10 and CCQD-X 1:50

Source: Authors' own data

https://doi.org/10.24191/mjcet.v8i2.4613

Table 3. CHNS elemental analysis of chitosan and freeze-dried CCQDs

Sample	Weight (mg)	Carbon%	Hydrogen%	Nitrogen%	Sulfur%
Chitosan	2.236	34.00	9.58	7.99	0.62
Freeze-dried CCQDs	1.760	6.38	3.36	4.62	1.09

Source: Author's own data

Table 3 shows the elemental composition of freeze-dried CCQDs and chitosan. The composition of freeze-dried CCQDs is 6.38% carbon and 3.36% hydrogen and chitosan contain larger amounts: 34.00% carbon and 9.58% hydrogen. Freeze-dried CCQDs contain a lesser amount of nitrogen (4.62%) compared to chitosan (7.99%). Nevertheless, the amount of sulfur is greater in the freeze-dried CCQDs (1.09%) when compared to chitosan (0.62%). When subjected to hydrothermal treatment, the organic components of chitosan are converted into carbon-based nanoparticles, and this is why there is a reduction in the levels of carbon and nitrogen in the final products of the CCQDs (Song et al., 2018). Increased amount of sulfur is the confirmation that thiourea, which is a sulfur containing dopant has been successfully incorporated into the CCQDs structure. The hydrogen content reflects surface functional groups like hydroxyl groups and amine groups which aid in promoting hydrophilicity and stability. The same trends are reported in the literature. Research by Cui et al. (2022) and Zhou et al. (2022) indicate that ejection of sulfur on CQDs through the use of thiourea increases the amount of sulfur on the surfaces. Sulfur doping increases the capacity of the CQDs to participate as electron donors and improves the surface properties, which makes them better in use as a CO 2 capture mechanism (Cui et al., 2022; Zhou et al., 2022). Chang et al. (2022) discovered that part of the nitrogen is lost in the thermal decomposition process, yet the rest of the nitrogen is used in the heteroatom doping of the CQDs- in line with the amount of nitrogen observed post-synthesis. Such doping enhances the adsorption capacity and chemical reactivity of CQDs, which is why they can be used in the environment (Chang et al., 2022).

3.4 Adsorption capacity of CCQD-X with varying CCQDs configurations

Different configurations of CCQDs were used to test the adsorption ability of this material. The paper examined the impact of concentration and phase of the CCQDs, including varying volumes of solution (2 mL, 10 mL and 100 mL) and freeze-dried CCQDs on the CO_2 adsorption capacity of CCQD-X. The findings demonstrate the impact of these variables on CO_2 adsorption efficiency and determine the optimum configuration that can be used to optimise the performance of CCQD-X. Fig. 9 illustrates the CO_2 breakthrough curves of the various CCQD-X samples and how the CO_2 concentration (C/Co) varies with time during adsorption. Table 4 summarises the important properties, including breakthrough time, breakthrough capacity, total adsorption time, and total adsorption capacity, and the CO_2 adsorption performance of each CCQD-X sample. These measurements allow determining the effectiveness of each sample in the process of CO_2 absorption under the conditions tested, which identifies performance differences based on the amount of xerogel synthesised and the mode of its preparation.

https://doi.org/10.24191/mjcet.v8i2.4613

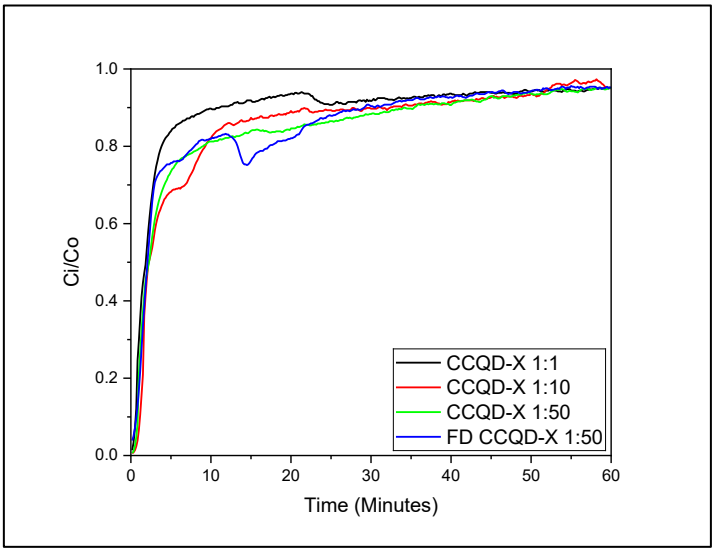

Fig. 9. CO_2 breakthrough curves for CCQD-X samples

Source: Author's own data

Table 4. CO_2 adsorption performance of CCQD-X samples

Samples	Breakthrough time (min)	Breakthrough capacity (mg/g)	Total adsorption time (min)	Total adsorption capacity (mg/g)
CCQD-X 1:1	0.67	0.9478	50.33	37.71
CCQD-X 1:10	1.17	0.9579	46.33	51.71
CCQD-X 1:50	1.00	1.1489	34.33	80.28
FD CCQD-X 1:50	0.83	0.9437	54.50	55.24

Source: Author's own data

A freeze-dried CCQDs sample (FD CCQD-X 1:50) and CCQD-X samples made with varying CCQDs-to-solution ratios (1:1, 1:10, and 1:50) are shown in Table 4 along with their CO_2 adsorption performance. The samples with the lowest breakthrough capacity (0.9478 mg/g) and the shortest breakthrough time (0.67 min) are CCQD-X 1:1, suggesting a limited initial adsorption ability and a faster saturation of adsorption sites. The lowest total capacity (37.71 mg/g) and the longest total adsorption time (50.33 min) indicate that this ratio is not ideal for CO_2 adsorption. With a slightly higher breakthrough capacity (0.9579 mg/g) and a longer breakthrough period (1.17 min), the CCQD-X 1:10 sample performs better. In contrast to the CCQD-X 1:1 sample, its total adsorption duration drops to 46.33 min, but its total adsorption capacity rises noticeably to 51.71 mg/g, suggesting improved CO_2 retention. Among the tested adsorbents, the CCQD-X 1:50 sample demonstrated the highest performance. It registered the best breakthrough capacity of 1.1489 mg/g at a breakthrough time of 1.00 min and achieved the highest total adsorption capacity of 80.28 mg/g over 34.33 min. This performance indicates the remarkable efficiency afforded by its optimal CCQD-to-solution ratio.

In comparison, the freeze-dried FD CCQD-X 1:50 sample showed more modest results, with a lower total capacity of 55.24 mg/g and a longer saturation time of 54.5 min. This comparative analysis suggests that while the freeze-dried CCQDs are effective, the suspension-based synthesis method is superior. It likely fosters a more advantageous pore morphology and a more homogeneous dispersion of the CCQDs within the xerogel matrix, leading to significantly enhanced adsorption efficiency. The comparatively lower performance of the FD CCQD-X 1:50 adsorbent can likely be attributed to the freeze-drying process itself.

https://doi.org/10.24191/mjcet.v8i2.4613

This method can induce aggregation of the CCQDs particles and lead to partial pore-blocking within the xerogel matrix. As a consequence, the accessibility of active sites for CO_2 binding is reduced, and the diffusion of gas molecules through the material is hindered (Andreana et al., 2023; Park, 2017).

CCQD-X 1:50 demonstrated a CO_2 adsorption capacity of 80.28 mg/g, which was higher than the maximum uptake of 48.5 mg/g obtained by the polyurethane (PU)/ionic silica xerogel composites by dos Santos et al. (2019). The difference can be explained by the differences in the chemical and physical properties of the adsorbents. The CCQD-X 1:50 sample has a t-plot micropore area of 0.2601 m^2/g and a BET surface area of 0.1864 m^2/g, which shows a mesoporous structure. Even though the surface area is not really large, the presence of both mesopores and micropores facilitates CO_2 adsorption. Also, the inclusion of heteroatoms like sulfur and nitrogen into the CQDs improves surface functionalities and CO_2 affinity. Such beneficial characteristics are probably created in part due to the hydrothermal synthesis procedure applied to CCQD-X 1:50 (dos Santos et al., 2019). Conversely, PU/ionic silica xerogel composites incorporate silica xerogels functionalised with room temperature ionic liquids (RTILs) in PU matrix. The specific surface areas of the composites differ based on the kind of functionalised xerogel and the quantity of the same that is incorporated. The composites with fluorinated RTILs had larger CO_2 sorption rates due to the presence of fluorinated anions, which increased specific surface areas and enhanced CO_2 affinity. Nevertheless, adding these xerogels to the PU matrix might lead to aggregation of the filler and the decreased total surface area that can be used in adsorption and the poor mechanical properties of the composites. The mesoporous architecture of CCQD-X 1:50, consisting of nitrogen and sulfur functional groups to enhance CO_2 contact, is probably synergistic in contributing towards its superior adsorption characteristic. In the meantime, while functionalised xerogels is advantageous to PU/ionic silica xerogel composites, their adsorption efficiency depends on the dispersion of fillers and their interaction with the matrix, challenges that the CCQD-X synthesis route appears to mitigate more effectively.

4. CONCLUSIONS

This study reveals that stabilisation of chitosan-based carbon quantum dots with a xerogel support is viable to remove CO_2. Xerogel matrix increases the surface area and maintains structural integrity of the xerogel during the adsorption process to offer the CCQDs a solid foundation which enhances its uptake. This plan sheds light on how developed support systems like xerogels paired up with renewable resources like chitosan can result in effective and permanent CO_2 capture systems. This study also concludes that the CCQD-X 1:50 sample had the best CO_2 adsorption capacity of 80.28 mg/g meaning that it has potential to be used as an effective adsorbent in capturing CO_2 in the environment. The mesoporous structure with significant adsorption properties is shown by the BET analysis: surface area 0.1864m^2/g, and t-plot micropore area 0.2601 m^2/g. In particular, the higher residual weight of 40% at 950°C of CCQD-X 1:1 is highly indicative of a strong carbon structure capable of operating under a variety of operating conditions which reflects the thermal stability of the samples. The analysis using FTIR proves the availability of functional groups like hydroxyl and amine that increase the interaction with CO_2. Besides, CHNS elemental analysis indicates that the carbon and nitrogen content decreases because of hydrothermal synthesis, whereas the sulfur doping enhances surface functionalities and total adsorption capacity.

ACKNOWLEDGEMENTS/FUNDING

This research was supported by the Ministry of Higher Education (MOHE) through the Fundamental Research Grant Scheme (Grant No. FRGS/1/2022/TK0/UITM/02/55). The authors are grateful for the facilities provided by Faculty of Chemical Engineering, Universiti Teknologi MARA (UiTM) Cawangan Pulau Pinang, Kampus Permatang Pauh to complete this work. The authors would like to express their deepest gratitude to all those who have provided the means and possibility for completing this work.

CONFLICT OF INTEREST STATEMENT

The authors agree that this research was conducted in the absence of any self-benefits, commercial or financial conflicts and declare the absence of conflicting interests with the funders.

AUTHORS' CONTRIBUTIONS

Nur Ainaa Mohd Hasyim Chan: Conceptualisation, methodology, formal analysis, validation, investigation and writing-original draft; **Norhusna Mohamad Nor**: Conceptualisation, supervision, methodology, writing- review and editing, formal analysis, writing- review and editing, and validation.

DATA AVAILABILITY

Data will be made available on request.

REFERENCES

Aguilar-Maruri, S. A., Perera-Triana, D., Flórez, E., Forgionny, A., Palestino, G., Gómez-Durán, C. F. A., & Ocampo-Pérez, R. (2024). Highly Adsorptive Organic Xerogels for Efficient Removal of Metformin from Aqueous Solutions: Experimental and Theoretical Approach. *Processes*, *12*(7), 1431. https://doi.org/10.3390/PR12071431

Alias, A. B., Qarizada, D., Malik, N. S. A., Noraini, N. M. R., & Rashid, Z. A. (2022). Comparison of hydrogel-and xerogel-based sorbent from Empty Fruit Bunch (EFB). *Archives of Materials Science and Engineering*, *118*(2), 49–60. https://doi.org/10.5604/01.3001.0016.2579

Andreana, I., Bincoletto, V., Manzoli, M., Rodà, F., Giarraputo, V., Milla, P., Arpicco, S., & Stella, B. (2023). Freeze Drying of Polymer Nanoparticles and Liposomes Exploiting Different Saccharide-Based Approaches. *Materials*, *16*(3), 1212. https://doi.org/10.3390/MA16031212/S1

Bahman, N., Alalaiwat, D., Abdulmohsen, Z., Al Khalifa, M., Al Baharna, S., Al-Mannai, M. A., & Younis, A. (2023). A critical review on global CO_2 emission: Where do industries stand? *Reviews on Environmental Health*, *38*(4), 681–696. https://doi.org/10.1515/REVEH-2022-0105/MACHINEREADABLECITATION/RIS

Boudouaia, N., Bengharez, Z., & Jellali, S. (2019). Preparation and characterization of chitosan extracted from shrimp shells waste and chitosan film: application for Eriochrome black T removal from aqueous solutions. *Applied Water Science*, *9*(4). https://doi.org/10.1007/S13201-019-0967-Z

Chang, K., Zhu, Q., Qi, L., Guo, M., Gao, W., & Gao, Q. (2022). Synthesis and Properties of Nitrogen-Doped Carbon Quantum Dots Using Lactic Acid as Carbon Source. *Materials*, *15*(2), 466. https://doi.org/10.3390/MA15020466

Chen, X., Liu, W., Sun, Y., Tan, T., Du, C. X., & Li, Y. (2023). KOH-Enabled Axial-Oxygen Coordinated Ni Single-Atom Catalyst for Efficient Electrocatalytic CO_2 Reduction. *Small Methods*, *7*(3), 2201311. https://doi.org/10.1002/SMTD.202201311

Cui, H., Xu, J., Shi, J., Yan, N., Zhang, C., & You, S. (2022). N, S co-doped carbon spheres synthesized from glucose and thiourea as efficient CO_2 adsorbents. *Journal of The Taiwan Institute of Chemical Engineers*, *138*, 104441. https://doi.org/10.1016/J.JTICE.2022.104441

Deana, Q., Nor Mohd, R. N., Azil, B. A., Hamasa, K., & Nurul, S. A. A. (2023). Adsorption of hydrogen sulphide (H_2S) using xerogel synthesized from palm kernel shell biochar. *Materials Research Proceedings*, *29*, 109–116. https://doi.org/10.21741/9781644902516-14

dos Santos, L. M., Bernard, F. L., Pinto, I. S., Scholer, H., Dias, G. G., Prado, M., & Einloft, S. (2019). Polyurethane /Ionic Silica Xerogel Composites for CO_2 Capture. *Materials Research-Ibero-American Journal of Materials*, *22*. https://doi.org/10.1590/1980-5373-MR-2019-0022

Friedlingstein, P., Houghton, R. A., Marland, G., Hackler, J., Boden, T. A., Conway, T. J., Canadell, J. G., Raupach, M. R., Ciais, P., & Le Quéré, C. (2010). Update on CO_2 emissions. *Nature Geoscience*, *3*(12), 811–812. https://doi.org/10.1038/NGEO1022

Gautam, & Sahoo, S. (2022). Experimental investigation on different activated carbons as adsorbents for CO_2 capture. *Thermal Science and Engineering Progress*, *33*, 101339. https://doi.org/10.1016/J.TSEP.2022.101339

Gong, W., Tao, C., Tian, Z., Huang, Z., Lin, H., Qi, C., Yu, Z., & Guo, L. (2025). Characterization and mechanism of phosphorus adsorption from wastewater by lanthanum calcium doped sludge/wheat straw biochar. *Frontiers in Environmental Science*, *13*, 1604542. https://doi.org/10.3389/FENVS.2025.1604542/BIBTEX

Hannachi, Y., Hafidh, A., & Ayed, S. (2019). Effectiveness of novel xerogels adsorbents for cadmium uptake from aqueous solution in batch and column modes: Synthesis, characterization, equilibrium, and mechanism analysis. *Chemical Engineering Research and Design*, *143*, 11–23. https://doi.org/10.1016/j.cherd.2019.01.006

Hao, W., Lee, S. H., & Peera, S. G. (2023). Xerogel-Derived Manganese Oxide/N-Doped Carbon as a Non-Precious Metal-Based Oxygen Reduction Reaction Catalyst in Microbial Fuel Cells for Energy Conversion Applications. *Nanomaterials*, *13*(22), 2949. https://doi.org/10.3390/NANO13222949/S1

Helmi, M., Moazami, F., Hemmati, A., & Ghaemi, A. (2023). Synthesis and characterization of KOH@Graphene oxide-Fe_3O_4 as a magnetic composite adsorbent for CO_2 capture. *Journal of Physics and Chemistry of Solids*, *178*, 111338–111338. https://doi.org/10.1016/J.JPCS.2023.111338

Kim, K. H., & Kim, M. H. (2023). Adsorption of CO_2, CO, H_2, and N_2 on Zeolites, Activated Carbons, and Metal-Organic Frameworks with Different Surface Nonuniformities. *Sustainability*, *15*(15). https://doi.org/10.3390/SU151511574

Kloos, R. L., Wineinger, D. M., & Weisshaar, D. E. (1999). QUANTITATIVE ANALYSIS OF A SOLID SOLUTION USING FOURIER TRANSFORM INFRARED SPECTROMETRY: AN INSTRUMENTAL ANALYSIS EXPERIMENT. In *Proceedings of the South Dakota Academy of Science* (Vol. 78).

Lamb, W. F., Wiedmann, T., Pongratz, J., Andrew, R., Crippa, M., Olivier, J. G. J., Wiedenhofer, D., Mattioli, G., Al Khourdajie, A., House, J., Pachauri, S., Figueroa, M., Saheb, Y., Slade, R., Hubacek, K., Sun, L., Ribeiro, S. K., Khennas, S., De La Rue Du Can, S., Chapungu, L., Davis, S.J., Bashmakov, I., Dai, H., Dhakal, S., Tan, X., Geng, Y., Gu, B., & Minx, J. (2021). A review of trends and drivers of greenhouse gas emissions by sector from 1990 to 2018. *Environmental Research Letters*, *16*(7), 073005. https://doi.org/10.1088/1748-9326/ABEE4E

Li, Y., Gong, D., Zhou, Y., Zhang, C., Zhang, C., Sheng, Y., & Peng, S. (2022). Respiratory Adsorption of Organic Pollutants in Wastewater by Superhydrophobic Phenolic Xerogels. *Polymers*, *14*(8), 1596. https://doi.org/10.3390/POLYM14081596

Mahdi, H. H., Saleh, A. M., Alias, A. B., Jawad, A. H., Salman, S. D., Qarizada, D., Mostafa, M. M., Saleh, N. M., & Abdulqader, M. A. (2024). Synthesis and Characterization of Xerogel Derived from Palm Kernel Shell Biochar and Comparison with Commercial Activated Carbon. *Journal of Ecological Engineering*, *25*(6). https://doi.org/10.12911/22998993/183719

Minx, J. C., Lamb, W. F., Andrew, R. M., Canadell, J. G., Crippa, M., Döbbeling, N., Forster, P. M., Guizzardi, Di., Olivier, J., Peters, G. P., Pongratz, J., Reisinger, A., Rigby, M., Saunois, M., Smith, S. J., Solazzo, E., & Tian, H. (2021). A comprehensive and synthetic dataset for global, regional and national greenhouse gas emissions by sector 1970-2018 with an extension to 2019. *Earth System Science Data*, *13*(11), 5213–5252. https://doi.org/10.5194/ESSD-13-5213-2021

https://doi.org/10.24191/mjcet.v8i2.4613

Nazir, G., Rehman, A., & Park, S. J. (2021). Role of heteroatoms (nitrogen and sulfur)-dual doped corn-starch based porous carbons for selective CO_2 adsorption and separation. *Journal of CO_2 Utilization*, *51*, 101641. https://doi.org/10.1016/j.jcou.2021.101641

Noraini, N. M. R., Alias, A. B., Qarizada, D., Azman, F. A. M., Rashid, Z. A., & Hasan, M. R. C. (2022). Synthesis and Characterization of Xerogel from Palm Kernel Shell Biochar. *Journal of Mechanical Engineering*, *11*(Special Issue 1), 211–226. https://doi.org/10.24191/jmeche.v11i1.23599

Olasehinde, E. F., & Abegunde, S. M. (2020). Preparation and characterization of a new adsorbent from *Raphia taedigera* seed. *Research on Engineering Structures and Materials*, *6*(2), 167–182. https://doi.org/10.17515/resm2019.139ma0713

Park, K. (2017). Prevention of nanoparticle aggregation during freeze-drying. *Journal of Controlled Release*, *248*, 153. https://doi.org/10.1016/j.jconrel.2017.01.038

Paul, A., & Kurian, M. (2021). Facile synthesis of nitrogen doped carbon dots from waste biomass: Potential optical and biomedical applications. *Cleaner Engineering and Technology*, *3*, 100103. https://doi.org/10.1016/j.clet.2021.100103

Sezgin, D. (2022). Xerogel of fast kinetics and high adsorption capacity for cationic dye removal. *Sigma Journal of Engineering and Natural Sciences*, 189–197. https://doi.org/10.14744/SIGMA.2022.00019

Shimizu, T., Kanamori, K., & Nakanishi, K. (2017). Silicone-Based Organic–Inorganic Hybrid Aerogels and Xerogels. *Chemistry – A European Journal*, *23*(22), 5176–5187. https://doi.org/10.1002/CHEM.201603680

Song, J., Zhao, L., Wang, Y., Xue, Y., Deng, Y., Zhao, X., & Li, Q. (2018). Carbon Quantum Dots Prepared with Chitosan for Synthesis of CQDs/AuNPs for Iodine Ions Detection. *Nanomaterials 2018, Vol. 8, Page 1043*, *8*(12), 1043. https://doi.org/10.3390/NANO8121043

Zhou, H., Ren, Y., Li, Z., He, W., & Li, Z. (2022). Selective Detection of Fe^{3+} by Nitrogen–Sulfur-Doped Carbon Dots Using Thiourea and Citric Acid. *Coatings 2022, Vol. 12, Page 1042*, *12*(8), 1042. https://doi.org/10.3390/COATINGS12081042

https://doi.org/10.24191/mjcet.v8i2.4613